JOURNAL OF BACTERIOLOGY, Sept. 2007, p. 6457–6468 Vol. 189, No. 17
0021-9193/07/$08.00+0 doi:10.1128/JB.00757-07

Spore Coat Architecture of *Clostridium novyi* NT Spores[▽]

Marco Plomp,[1] J. Michael McCaffery,[2] Ian Cheong,[3] Xin Huang,[3] Chetan Bettegowda,[3] Kenneth W. Kinzler,[3] Shibin Zhou,[3] Bert Vogelstein,[3]* and Alexander J. Malkin[1]*

Department of Chemistry, Materials and Life Sciences, Lawrence Livermore National Laboratory, L-234, Livermore, California 94551[1]; Department of Biology, Johns Hopkins University, 3400 N. Charles St., Baltimore, Maryland 21218[2]; and The Howard Hughes Medical Institute and the Ludwig Center for Cancer Genetics and Therapeutics at The Johns Hopkins Sidney Kimmel Comprehensive Cancer Center, 1650 Orleans Street, CRB1, Baltimore, Maryland 21231[3]

Received 14 May 2007/Accepted 14 June 2007

Spores of the anaerobic bacterium *Clostridium novyi* NT are able to germinate in and destroy hypoxic regions of tumors in experimental animals. Future progress in this area will benefit from a better understanding of the germination and outgrowth processes that are essential for the tumorilytic properties of these spores. Toward this end, we have used both transmission electron microscopy and atomic force microscopy to determine the structure of both dormant and germinating spores. We found that the spores are surrounded by an amorphous layer intertwined with honeycomb parasporal layers. Moreover, the spore coat layers had apparently self-assembled, and this assembly was likely to be governed by crystal growth principles. During germination and outgrowth, the honeycomb layers, as well as the underlying spore coat and undercoat layers, sequentially dissolved until the vegetative cell was released. In addition to their implications for understanding the biology of *C. novyi* NT, these studies document the presence of proteinaceous growth spirals in a biological organism.

Clostridium novyi is a motile, spore-forming, gram-variable (gram positive in young cultures, often gram negative in older cultures) anaerobic bacterium. It can cause infections leading to gas gangrene in humans, particularly after traumatic wounds or illicit drug use, and can also infect domestic animals, particularly sheep (22). The pathology of *C. novyi* is attributed to the lethal alpha-toxin (6). To reduce systemic toxicity, an attenuated strain, called *C. novyi* NT and devoid of the alpha-toxin, was generated. Intravenous injection of *C. novyi* NT spores into tumor-bearing mice was found to successfully eradicate large tumors, either in combination with radiation therapy (7) and chemotherapy (13) or by itself, since it can induce a potent immune response (1). When *C. novyi* NT spores are injected into mice, the spores exclusively germinate in tumors and spare other tissues, even in aged animals or those with ischemic myocardial lesions (16).

C. novyi NT is therefore one of the most promising bacterial agents for cancer therapeutics that have been described in the past few years (55). Such therapeutic approaches were first attempted more than 50 years ago and have continued sporadically since that time. Many of these attempts used various strains of clostridia. Despite this long history and the importance of clostridia spores in other medical contexts, there have been relatively few studies of either the nature of the germination and outgrowth processes or the structure of the spore coat. Germination is a well-defined process of conversion of a dormant spore into a metabolically active form (46). The outgrowth stage starts with the initiation of spore metabolism. During the outgrowth stage, macromolecular synthesis in the spore converts the germinated spore into a growing cell (35, 46). The spore coat endows bacterial spores with remarkable resistance to physical and chemical agents and allows them to persist in nature for centuries (11, 17, 57).

Atomic force microscopy (AFM) has been used to study the architecture and assembly of a wide range of biological systems (18, 20, 23, 24, 27, 34, 37, 45). We have recently demonstrated the capability of AFM to probe native spore coat structures of various *Bacillus* spp. at the nanometer scale (38, 39), their responses to environmental changes (38, 40), and the structural dynamics of single germinating spores (41). In the present study, we use a combination of AFM and conventional transmission electron microscopy (TEM) ultrathin sectioning to probe the assembly of the spore coat of *C. novyi* NT spores. We have developed procedures for chemical and physical dissection of the spores, revealing the spore coat crystalline layers. Finally, AFM-based dynamic germination experiments allowed us to reconstruct the complete architecture of the spore coat. All of the structures observed with AFM could be related to features seen in EM section images, thus establishing the first model for the structure of *C. novyi* NT spores.

MATERIALS AND METHODS

Spore preparation and purification. Spores were prepared essentially as described previously (13). Briefly, *C. novyi* NT was cultured in sporulation medium for at least 2 weeks to ensure a maximum yield of mature spores. Spores were then purified through two consecutive continuous Percoll gradients followed by four washes and resuspensions in phosphate-buffered saline. The purity of the spore preparations was determined to be >99.9% by phase-contrast microscopy, as well as by light microscopy after staining with malachite green and eosin Y (http://pb.merck.de/servlet/PB/show/1235100/115942en.pdf).

RNA stains. Spores or vegetative bacteria were dropped onto microscopic slides and heated at 50°C for 5 min. The spores/cells were fixed in 4% paraformaldehyde (Sigma-Aldrich) for 5 min. After a brief rinse with water, the spores or cells were permeabilized for 5 min with 1% Igepal CA-630 (Sigma-Aldrich).

* Corresponding authors. Mailing address for B. Vogelstein: The Howard Hughes Medical Institute and the Ludwig Center for Cancer Genetics and Therapeutics at The Johns Hopkins Sidney Kimmel Comprehensive Cancer Center, 1650 Orleans Street, CRB1, Baltimore, MD 21231. Phone: (410) 955-8878. Fax: (410) 955-0548. E-mail: vogelbe@welch.jhu.edu. Mailing address for A. J. Malkin: Department of Chemistry, Materials and Life Sciences, Lawrence Livermore National Laboratory, L-234, Livermore, CA 94551. Phone: (925) 423-7817. Fax: (925) 422-2041. E-mail: malkin1@llnl.gov.

▽ Published ahead of print on 22 June 2007.

The cells were then stained with SYBR green II (Molecular Probes, Eugene, OR), diluted 10,000-fold from the stock solution. After a brief rinse with water, the spores or cells were visualized via fluorescence microscopy.

Electron microscopy. Conventional TEM using ultrathin sections was performed essentially as described previously (7). For environmental scanning electron microscopy (ESEM), *C. novyi* NT spores were fixed in a solution containing 3% formaldehyde, 1.5% glutaraldehyde, and 100 mM cacodylate buffer (pH 7.4) for 1 h at room temperature. Spores were subsequently washed three times in double-distilled H_2O, deposited onto 25-mm cellulose nitrate filter circles, and either (i) allowed to air dry for 2 h prior to imaging using the large field detector at a relative humidity of <3% (20°C at 75 Pa) at 1.75 kV or (ii) observed at a relative humidity of ~95% (20°C with a chamber pressure of 2,000 Pa) using the gaseous secondary electron detector at 20 kV. Spores were observed and images recorded with a FEI Quanta 200 ESEM (FEI, Hillsboro, OR) at a specimen working distance of 4.5 mm.

AFM in air. Droplets of ~2.5 μl of *C. novyi* NT spore suspensions (10^8 to 10^9 spores/ml) were deposited on plastic coverslips and incubated for 10 min, after which the sample substrate was either carefully rinsed and allowed to dry or directly dried without rinsing; the use of either method produced similar results. Images were collected by using a Nanoscope IV atomic force microscope (Veeco Instruments, Santa Barbara, CA) operated in tapping mode. For imaging in air, Veeco, Olympus, and NanoWorld etched silicon tips with force constants of ~40 N/m and resonance frequencies of ~300 kHz were used. Tapping amplitude, phase, and height images were collected simultaneously. Height images were primarily used for quantitative measurements, and amplitude and phase images were used predominantly for presentation.

Removal of amorphous outer spore coat layer. To analyze the spore coat architecture, the amorphous outer layer ("shell") was removed by chemical or physical means. The chemical treatments included incubations in 8 M urea, 10% sodium dodecyl sulfate (SDS), 15 mM dithiothreitol (DTT) with 2% SDS, 4 to 10% 2-mercaptoethanol with 2% SDS, 3 M urea–4% 2-mercaptoethanol–2% SDS, or 2% SDS plus DTT at concentrations ranging from 0.1 to 20 mM. The spore suspensions were exposed to these agents for a total of 1 h at 40°C in a Eppendorf Thermomixer R (Eppendorf North America, Westbury, NY) at 300 rpm. During this hour, there were three 2-min interruptions for vortexing at room temperature. Afterward, the spore suspensions were sonicated for five minutes in a 150-W sonicator (Branson; Ultrasonics Co., Danbury, CT) cooled with ice water. Vortexing and sonication were performed to shed the remnants of the digested amorphous material from the spores. Finally, the spore suspensions were washed three times with water to remove chemicals and prepared for imaging as described above. Note that sonication alone, without chemical treatment, proved insufficient to remove all amorphous material, even when the sonication was performed with a more powerful sonicator (400W Branson 450D) and a sonication time increased to 45 min.

Alternatively, a French press (Thermo Scientific, Waltham, MA), equipped with a 4-ml mini cell, was used with an operation pressure of 20K PSI to strip the spores of their amorphous shell. In this procedure, *C. novyi* NT spore suspensions were diluted with water to 4 ml before being placed in the mini cell and were reconcentrated afterward to reach a sufficiently high concentration for AFM visualization. This procedure resulted in the removal of the outer amorphous shell without any additional treatment.

Germination and outgrowth. Optimal in vitro germination conditions for *C. novyi* NT spores were evaluated by optical phase-contrast microscopy with a ×100 objective lens (Eclipse 50i; Nikon USA, Melville, NY). To gauge the impact of heat activation, the spore suspensions were heated for 30 min at 60 to 90°C in an Eppendorf Thermomixer R at 300 rpm prior to germination. Heat-activated spore suspensions were added to Bagadi germination medium (4, 12), supplemented with Oxyrase For Broth (Oxyrase, Mansfield, OH), which removes oxygen from solution, thereby enabling germination outside an anaerobic chamber. Germination itself was conducted in Eppendorf tubes in an incubator at 37°C. Droplets of 2 μl were removed at predetermined intervals and examined for germination and outgrowth progress (i.e., the number of phase-dark spores and vegetative cells) by using phase-contrast microscopy.

For AFM-based germination experiments, the *C. novyi* NT spores were stripped from the amorphous shells by using a French press and heat-activated for 30 min at 70°C. A 2.5-μl droplet of spore suspension was deposited onto a plastic coverslip, incubated for 10 min, and then carefully rinsed and placed in the AFM fluid cell (Veeco Instruments). This cell was equipped with a thermocouple and a temperature controller (Veeco Instruments Multimode heater package) with an operating range of ambient temperature to 60°C. The fluid cell was filled with deoxygenating Oxyrase-enriched Bagadi germination medium that was refreshed every 3 h, while the temperature was maintained at 37 ± 0.5°C. For AFM imaging in liquid, Veeco Instruments and Olympus silicon nitride cantilevers (force constant of 0.1 N/m) with either etched silicon or oxide-sharpened silicon nitride tips were used. In AFM-based germination experiments, light tapping-mode imaging was utilized exclusively in order to minimize tip-induced effects on the coat structure of germinating spores (41). The imaging force during experiments was carefully controlled and/or adjusted in order to avoid possible tip-induced artifacts (41).

RESULTS

TEM of ultrathin sections. Ultrathin sections of intact *C. novyi* NT spores reveal the dark spore core, surrounded by a thick, electron-transparent cortex and a multilayered spore coat (Fig. 1). Between the spore core and cortex, an electron-translucent germ cell wall is often seen (Fig. 1c). The cortex has dark-stained granules at its outer edges (Fig. 1b). The border region between the cortex and the spore coat, which we define as the undercoat (Fig. 1b), is formed by a 4- to 8-nm dark layer facing the cortex, a 6- to 8-nm gray layer facing the spore coat, and a 8- to 10-nm light layer sandwiched in between. The ~25- to 50-nm thick spore coat is formed typically by four to seven layers, each of which is 5 to 7 nm thick (Fig. 1b). As seen in Fig. 1a, most spores are surrounded by large swaths of amorphous material that we label as amorphous shells or, more simply, shells. These shells can occupy a large volume around the spores, in many cases more than 100% of the spore volume itself. Smaller amorphous shells (thickness, ~100 to 200 nm) are usually more or less concentric around the spore, while larger shells (thickness, ~200 to 400 nm) tend to have most of their volume beyond one or two of the spore's poles, extending up to 1 μm in length (Fig. 1a). In most cases the amorphous shells seem contained on their outer edge. Sometimes, spores and/or amorphous material were found to be contained within a 50- to 100-nm-thick sacculus (Fig. 1a).

In most spores, the amorphous shell contains a sizable number of thin, ordered paracrystalline layers (Fig. 1c to f), which are frequently attached to the spore coat and are found as well within the amorphous shell or near its outer surface. Some amorphous material sandwiched between the spore coat and the paracrystalline layer (e.g., gray arrow in Fig. 1e) was often observed. The paracrystalline layers, which were usually oriented parallel to the spore coat, are mostly single sheet, with a thickness of 8 ± 1 nm and an apparent lateral periodicity of 15 ± 1 nm. Occasionally, they formed assemblies of double layers (Fig. 1f).

AFM observations of surface morphology of air-dried *C. novyi* NT spores. AFM images of deposited, rinsed, and air-dried *C. novyi* NT spores confirmed that the spores were encased in amorphous shells (Fig. 2a and b). Many spores exhibited ~200-nm-thick shell "tails" at their poles (Fig. 2a and b) similar to "tails" visualized by TEM (Fig. 1a). High-resolution AFM images reveal that the outer shell surface typically consists of irregular amorphous material (Fig. 2c). On some spore surfaces, small areas of a highly regular honeycomb layer with a hexagonal symmetry and a periodicity of 8.7 ± 1 nm were observed (Fig. 2c).

Note that the process of drying did not alter the morphology of *C. novyi* NT spores, as shown through the use of ESEM (Fig. 2d and e).

When droplets of spore suspensions were not rinsed after incubation on the substrate but left to dry completely, a substantial amount of 20- to 30-nm thick and up to 6-μm-long

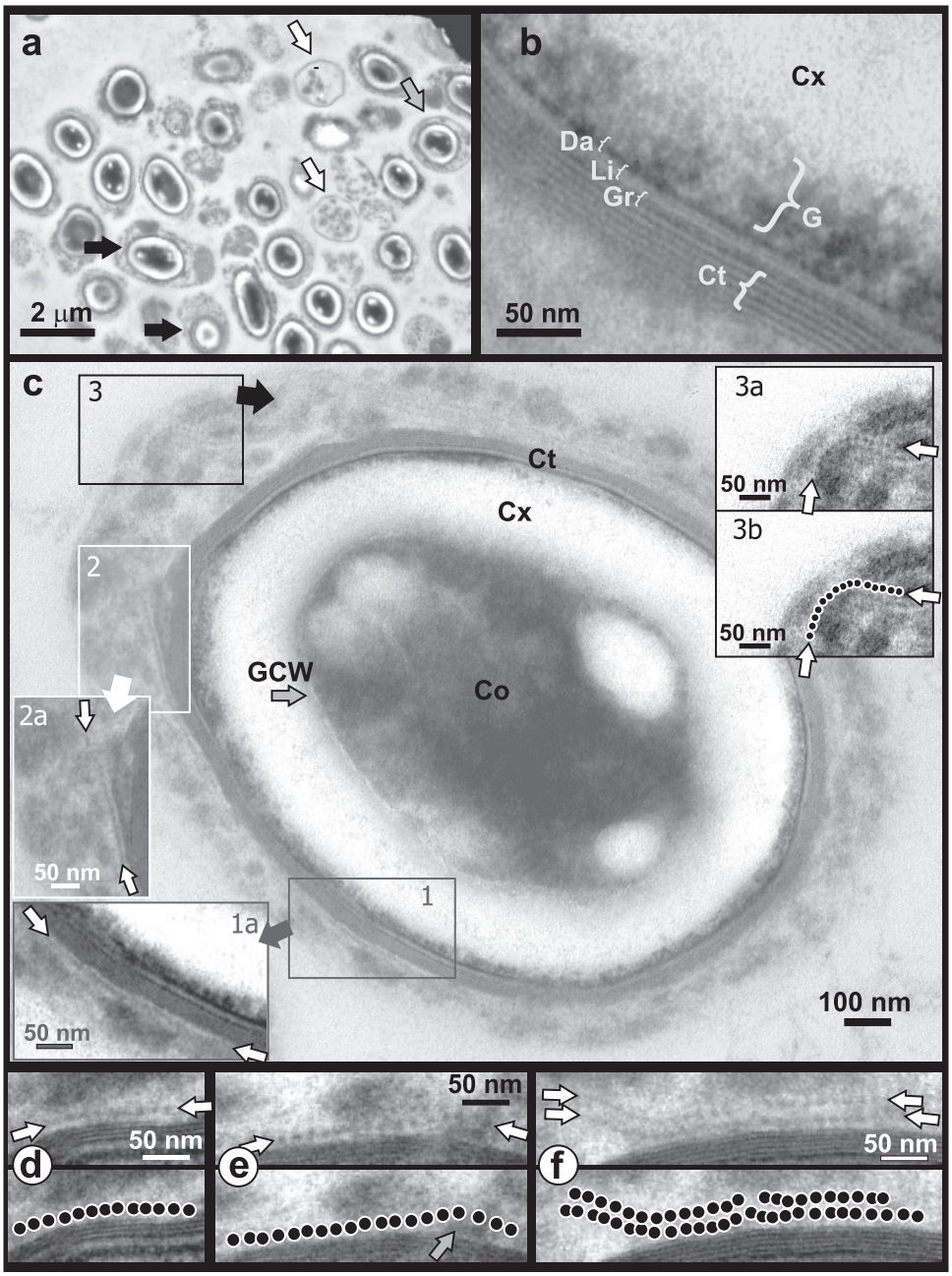

FIG. 1. TEM sections of *C. novyi* NT spore suspension. (a) Overview showing spores with dark core, and white cortex. All spores are surrounded by amorphous shells. Black arrows indicate spores with large shells, while gray and white arrows show spore-filled and empty sacculi, respectively. (b) Detail of the spore coat, showing five to seven coat layers (Ct), as well as a gray (Gr), light (Li), and dark (Da) layers forming the undercoat. The light-staining cortex (Cx) has dark-stained granules at its outer edges (G). (c) Between the core (Co) and cortex (Cx), a lightly stained germ cell wall (GCW, gray arrow) is often seen. The amorphous layer is intersected by thin sheets of ordered paracrystalline material, as highlighted for regions 1 to 3 in insets 1a to 3a and in panels d to f with small white arrows. (c, inset 1a) Ordered, paracrystalline layer positioned directly on the spore coat. (c, inset 2a) Paracrystalline layer partly attached to the spore coat, partly residing inside the amorphous layer. (c, inset 3a) Paracrystalline layer near the outside of the amorphous shell. (d to f) Additional examples of single (d and e) and double (f) paracrystalline layers (top). The periodic character of the paracrystalline layer is indicated in (c, inset 3b) and (d to f, bottom) with filled circles. Gray arrow in panel e (bottom panel) points to amorphous material sandwiched between the paracrystalline layer and the spore coat.

fibers were found on the substrate (data not shown). Some of these seemed to be associated with spores. These fibers were never seen on rinsed samples. This led us to speculate that these fibers are loose flagellum remnants originating from the vegetative phase.

Spore coat architecture. To observe the structure of the spore coat beneath the amorphous shell, we developed procedures to remove the shells by chemical treatment with various reducing agents and detergents or by physical treatment using a French press. Both procedures resulted in the removal of the

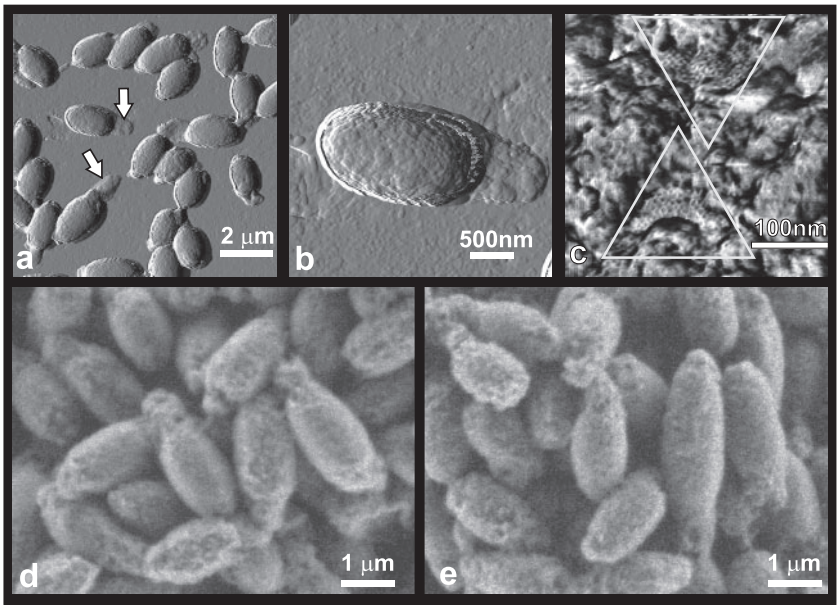

FIG. 2. (a to c) AFM images of air-dried *C. novyi* NT spores. (a) Amplitude image showing tails (arrows) corresponding to the amorphous shells; (b) amplitude image of a single spore showing the irregular spore surface and a "tail"; (c) phase image showing the irregular, amorphous shell surface in detail. Two smaller patches of crystalline honeycomb layer with a periodicity of ~8.7 nm are seen (inside triangles). (d and e) ESEM analysis of wet *C. novyi* NT spores revealed minimal differences in surface morphology compared to that of dry spores. *C. novyi* NT spores presented a highly varied, rough and/or irregular surface when viewed dry (<3% relative humidity) (d) or at ~95% relative humidity (e).

amorphous shell. As illustrated in Fig. 3, treated spores possess neither the 'tails' nor the irregular surface typical of intact spores (Fig. 2a to c) and instead show a wrinkled spore coat structure (Fig. 3a and c), which is typical of dried bacterial spores (39, 40). Similarly, TEM of ultrathin sections of *C. novyi* NT spores treated with 8 M urea (Fig. 3b) reveal the removal of the amorphous shell seen in TEM images of intact spores (Fig. 1a and c). Note that partially destroyed sacculi (Fig. 3b) are not seen in AFM images of chemically treated spores (Fig. 3a and c). This is most likely due to the sacculi's disintegration during the sonication step performed at the sample preparation for AFM imaging.

Approximately 15% of the spores stripped of the amorphous shell by French press appear to have damaged internal structures, which results in their partial collapse after they were dried on the substrate (data not shown). For both French-pressed and chemically treated spores, a small percentage of spores have a smooth appearance (Fig. 3c). These spores may have been stripped of all of their honeycomb and coat layers, revealing the undercoat or cortex layers.

When either French press or relatively mild reducing treatments (2 to 10% mercaptoethanol–2% SDS or 100 nM DTT–2% SDS) were used, the majority of the exposed spore surface is formed by an approximately 8- to 10-nm-thick honeycomb layer with a periodicity of 8.7 ± 1 nm (Fig. 3d and e), while part of the surface is still covered with amorphous remnants. In most cases, the honeycomb layers, while smooth themselves, appear to be folded on top of some underlying structure (Fig. 3d and e). This indicates that there is some (amorphous) material sandwiched between the honeycomb layer and the underlying spore coat layers, a finding consistent with the TEM data (Fig. 1f).

When intact spores were treated with harsher conditions (20 mM DTT, 2% SDS) a honeycomb-like pattern that was composed of separate building units was found (Fig. 3f). Individual units were 6 to 8 nm long and 1 to 2 nm wide. This pattern likely represents a partial degradation of the original honeycomb structure due to the increased amount of reducing agent used. Treatment of intact spores with 8 M urea resulted not only in the removal of the amorphous shell but also in the partial disintegration of the honeycomb layer (Fig. 3g). Furthermore, the harsh combination of 3 M urea, 4% 2-mercaptoethanol, 40 mM DTT, and 2% SDS resulted in the partial removal of the honeycomb layer, which revealed an underlying multilayered structure formed by ~6-nm-thick, smooth layers (Fig. 3h).

Germination and outgrowth of *C. novyi* NT spores. In preliminary AFM experiments, we found that spores with amorphous shells did not adhere well to the substrate and could not be imaged with a satisfactory resolution and that spores treated with a French press adhered better and could be reliably imaged. Moreover, in both cases only a relatively small fraction of spores proceeded to the outgrowth stage, which took many hours and hampered successful AFM imaging. In order to increase the percentage and speed of germinating spores, we evaluated the influence of heat activation on the germination and outgrowth of *C. novyi* NT spores. For this, 1.5-ml tubes containing 10 μl of *C. novyi* NT spore suspensions were incubated for 0.5 h at different temperatures ranging from 60 to 90°C, followed by incubation at 37°C with germination medium. The progress of the germination and outgrowth process was determined by analyzing 1-μl aliquots of the culture at 1-h intervals. The percentages of germinated (phase-dark) spores and emerging vegetative cells in the aliquots were determined

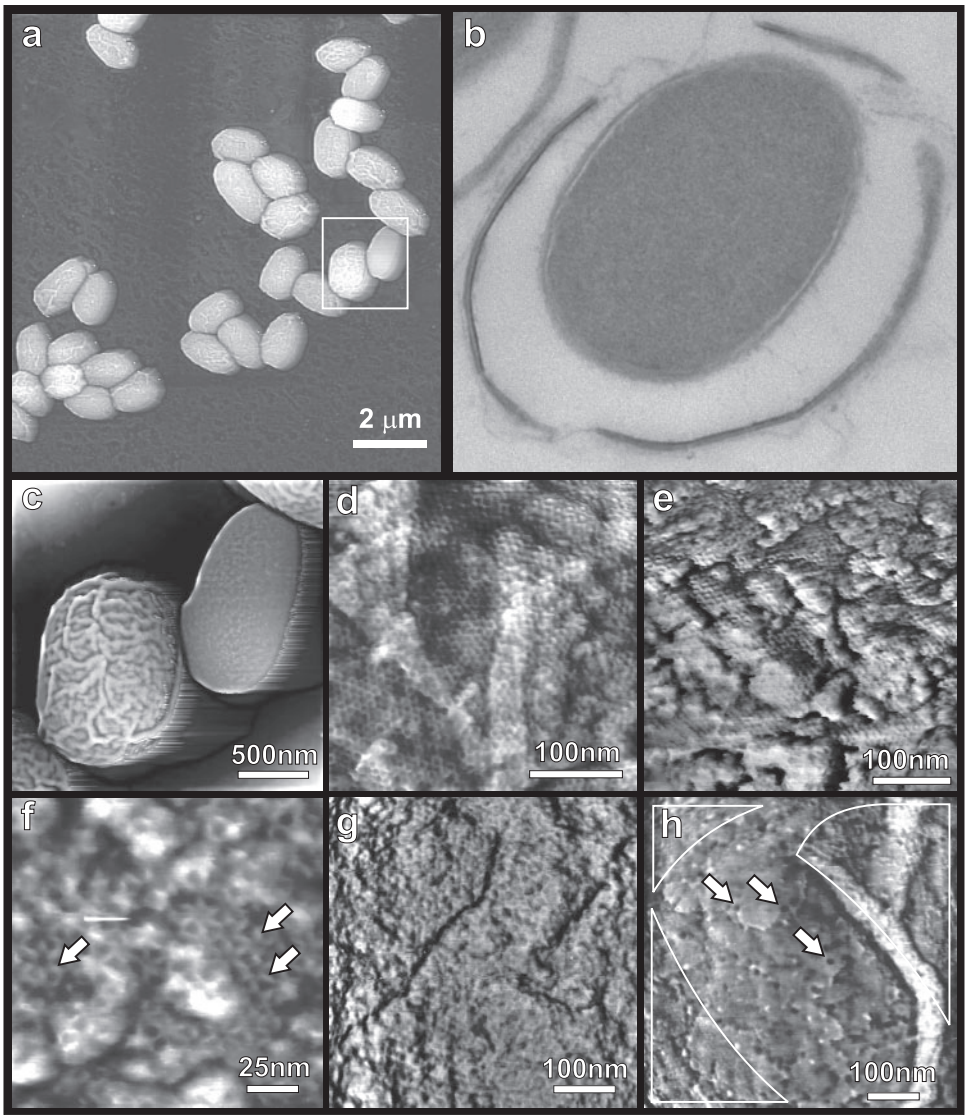

FIG. 3. Chemically treated and physically treated *C. novyi* NT spores. (a) Treatment of spores with 2% SDS–2% 2-mercaptoethanol resulted in the removal of the amorphous shell and, hence, in smoother spores. Most spores had a wrinkled appearance. (b) TEM section image of a spore treated with 8 M urea. The amorphous material is degraded, leaving an empty capsule around the clean spore. (c) The area indicated by the white square in panel a shows a heavily wrinkled spore, as well as a rare ultrasmooth spore. (d) Detailed observation of mildly treated spores (100 nM DTT–2% SDS) demonstrates that most spores are covered with honeycomb layers with ~8.7-nm periodicity. (e) Treatment with a French press similarly resulted in removal of the amorphous shell and exposure of a honeycomb layer. In both panels d and e, the thin, smooth honeycomb layers are seen to cover underlying irregular structures, probably amorphous material captured between the honeycomb layer and the spore coat. (f to h) Harsher chemical treatments of *C. novyi* NT spores. (f) For spores treated with 2% SDS–20 mM DTT, the honeycomb pattern was degraded into a pattern composed of separate building units (indicated by arrows) arranged in a triangular pattern. (g) Treatment of spores with 8 M urea degraded the honeycomb layer further, leaving its periodic nature barely visible. (h) Treatment with the combination of 3 M urea with 2% SDS, 4% 2-mercaptoethanol, and 40 mM DTT resulted in the partial removal of the honeycomb layer, which revealed an underlying layered structure (center). Arrows indicate ~15-nm holes in this layered structure. Remnants of the degraded honeycomb layer are indicated in white contours at the periphery of the image. Shown are height (a, c, d, f, and h) and phase (e and g) AFM images.

by phase-contrast microscopy. Without preceding temperature activation, only ~25% of the spores had germinated after 6 h (Fig. 4a), and only ~5% of spores proceeded to release vegetative cells at this time (data not shown). This was consistent with preliminary AFM experiments. As shown in Fig. 4a, we found that temperature activation significantly increased the percentage of germinating spores. Thus, 0.5 h activation at 60, 70, 80, and 90°C resulted in an increase of germination at 6 h to 45, 75, 90, and 65% of the spores, respectively. Furthermore, approximately 20 to 50% of heat-activated spores proceeded to outgrowth and released vegetative cells 6 h into incubation with germination medium (data not shown). Note that the decreased germination rate after 90°C activation is likely caused by an increased rate of killing of the spores during activation. Killing of spores at this temperature was reported for other spore species (44, 47).

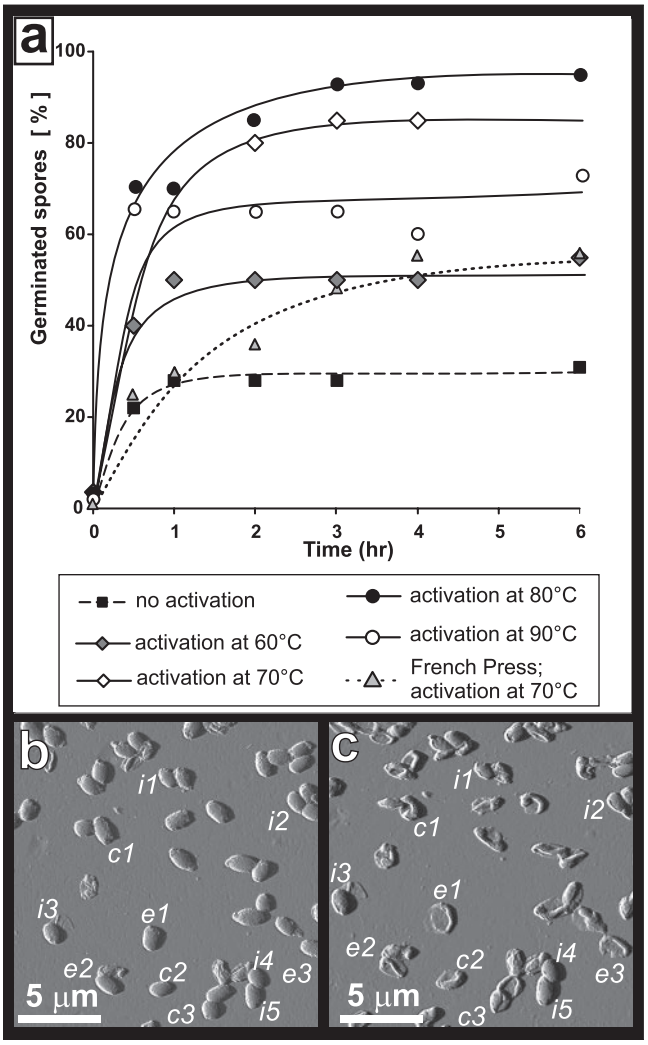

FIG. 4. *C. novyi* NT spore germination and outgrowth. (a) Impact of heat activation, at the indicated temperatures, on spore germination, as determined by phase-contrast microscopy. Trendlines were added for ease of viewing. (b and c) Spores were treated with a French press and then heat activated and exposed to germination medium. The same 18-by-18-μm^2 area imaged before (b) and after (c) a 24-h exposure to the germination medium (AFM amplitude images). Shown are spores that remained intact (*i1. . .i5*), that collapsed after germination (*c1. . .c3*), or that had fully outgrown, in which case only an empty spore coat is left (*e1. . .e3*).

Based on these adhesion and activation data, we chose to perform AFM germination and outgrowth experiments with French-pressed spores that were heat activated for 0.5 h at 70°C. For these (French-pressed) spores, the germination rate was lower than that of nonstripped spores with the same heat activation (Fig. 4a). Nevertheless, there were enough germinating spores to allow us to monitor the germination process at a high-resolution, single-spore level.

In AFM single spore germination experiments, we typically focused on a small group of neighboring spores. We then monitored their germination and outgrowth processes, starting at their first exposure to the germination medium and continuing until their release of vegetative cells. Since this approach allowed us to study only a few spores per experiment, we performed a control for each germination AFM experiment. Prior to exposure of substrate-adhered spores to germination medium, we imaged a large substrate area (typically 80 by 80 μm^2) containing a significant number of spores (Fig. 4b) and imaged the same area after the experiment, i.e., after 6 to 24 h of exposure to germination medium and subsequent rinsing and drying (Fig. 4c). This approach allowed us to evaluate the fate of a statistically relevant number of spores during the germination experiment. Thus, in the case of the experiment shown in Fig. 4, a total of ~800 spores were visualized on a 80-by-80-μm^2 area of the substrate prior to and after the germination experiment (shown in Fig. 4 b and c is a 18-by-18-μm^2 area part of this larger 80-by-80-μm^2 area). We found that after French press treatment, 0.5 h of activation at 70°C, and 24 h of germination at 37°C, ~10% of the spores remained intact; ~50 to 60% germinated but did not produce vegetative cells (as judged from their collapse upon drying, which is caused by replacement of spore inner structures with water upon germination); and approximately 30 to 40% proceeded to outgrowth, producing vegetative cells and leaving empty coats adsorbed on the substrate. The vegetative cells released into the solution are typically rinsed away during the washing step before imaging of the air-dried spore sample commences.

After onset of germination medium exposure, the quickest observable AFM timeframe for probing the high-resolution structure of single spores was about 15 to 20 min. By that time, we found that the spores often had partly or completely lost their honeycomb layers, revealing the underlying layers (Fig. 5a). The remaining patches of honeycomb layer were loosely attached to the underlying layer and could be easily removed by the AFM tip upon scanning with a slightly increased force (data not shown).

The removal of the honeycomb layer revealed a multilayer structure formed by ~6-nm-thick smooth layers (Fig. 5). Typically, there were three to six layers exposed on the spore surface. Both the number of these layers and their thickness were consistent with the spore coat layers (Fig. 1b) as seen in the TEM transverse sections. The spore coat surface patterns (Fig. 5b to d) were very similar to ones observed on the surfaces of inorganic, organic, and macromolecular crystals (14, 32, 33, 42). As seen in Fig. 5b to d, these crystalline spore coat layers appear to be generated on screw dislocations, which are a major growth source of conventional and macromolecular crystals. In the middle of the growth centers, the dislocations cause depressions, typically <15 nm, which are known as hollow cores in crystal growth theory and are formed by the stress associated with the dislocations (10, 15, 54).

Although AFM resolution is typically sufficient for visualization of crystal lattices on a molecular scale for a wide range of protein crystals (29, 33, 52), we were not able to resolve a regular, crystalline lattice on the *C. novyi* NT spore coat layers. Because the occurrence of steps and screw dislocations clearly points to the crystalline nature of these layers, we conclude that the plane lattice parameters are likely smaller than 1 nm, which is below our AFM resolution.

At later stages of the outgrowth process, the spore coat layers start to dissolve (Fig. 6). This process was initiated by the formation of fissures (Fig. 6a), which subsequently widened and elongated (Fig. 6b to e), resulting in isolated islands of

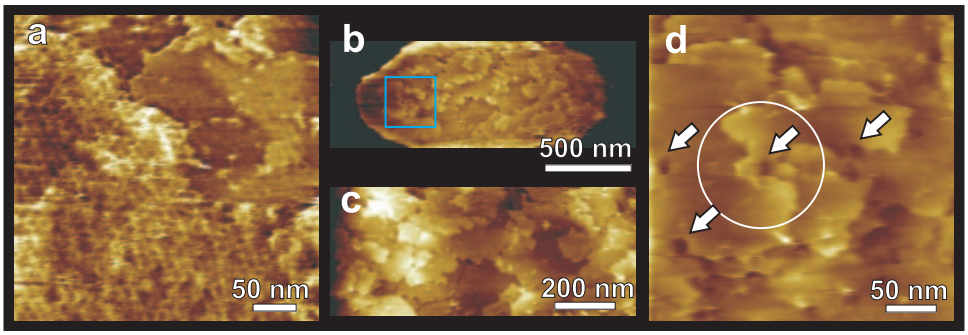

FIG. 5. *C. novyi* NT spore coats: high-resolution AFM height images. Spores were activated and exposed to germination medium as described in the text. (a) Most of the honeycomb layers disappeared from the spores within ~1 h. Remaining honeycomb patches (left, lower sides) could be easily removed by scanning with increased force. Below the honeycomb layer several underlying coat layers (upper right) are revealed. (b to d) Typical growth patterns seen on *C. novyi* NT spore surface after removing the honeycomb layers. (b) Whole spore with several ~6-nm-thick layers exposed on the surface. (c) Zoom-in of the center of panel b showing that spore coat layers originate at screw dislocations. (d) Zoom-in of the area indicated in panel b. The circle in panel d denotes a fourfold screw axis. Many dislocation centers show depressions reminiscent of hollow cores (arrows), which are found in a wide range of crystals. The times in germination medium (hours:minutes) were 5:40 (a) and 4:10 (b to d).

remnant coat layers (Fig. 6e and f). The dissolution of coat layers revealed an underlying undercoat layer (marked with arrows in Fig. 6e). At the final stages of outgrowth, the coat layers dissolved completely (Fig. 7a), fully exposing the undercoat layer. In the following stage of outgrowth this layer also disintegrated. This proceeded through the formation and slow expansion of ~25-nm-deep flat-bottom apertures (Fig. 7). Hence, the thickness of this undercoat layer was determined to be ~25 nm. A new layer, with a markedly rough surface, could be seen through the apertures (Fig. 7d). As time elapsed, it became clear that this new layer was the cell wall of the newly emerging vegetative cell. AFM phase imaging, which allows probing variations in adhesion, friction, hardness, and viscoelalasticity (30), showed that the cell wall layer was contrasted with respect to the surrounding spore coat material, indicating its distinctly different physicochemical properties (Fig. 7f). At the very last stage of outgrowth, the newly formed vegetative cell emerged from the spore coat and was released into the germination medium.

The spore coat degradation process presented in Fig. 5 to 7 appears not to be affected by the scanning AFM tip. The shapes of fissures and apertures remained unaltered after repeated scanning. Furthermore, when we zoomed out to a larger previously nonscanned area after prolonged scanning on a smaller spore area, the initially scanned area did not display any tip-induced alterations (such as a larger degree of coat

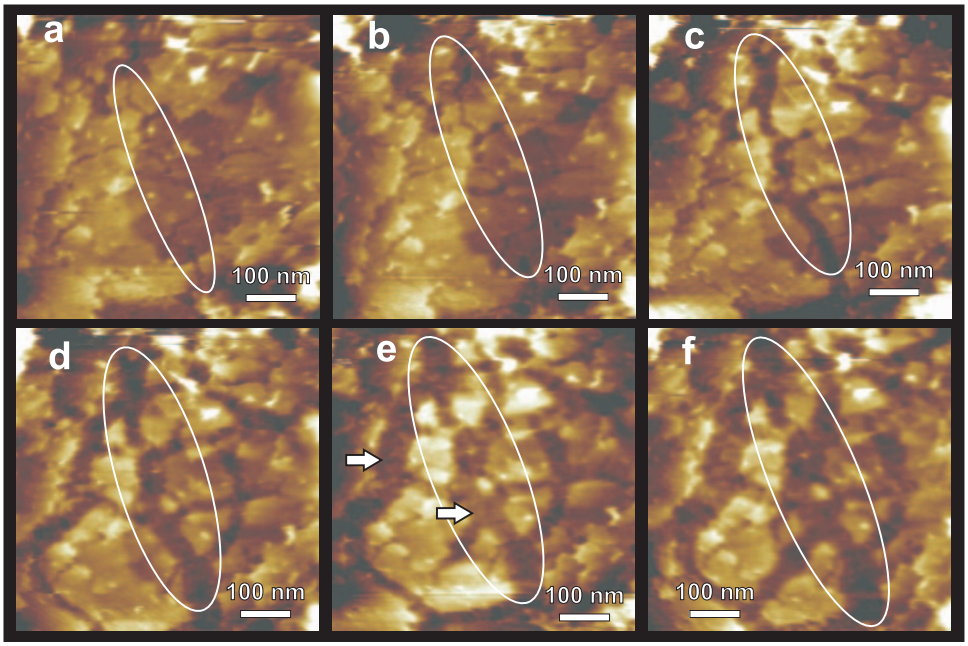

FIG. 6. Dynamic AFM height imaging of degrading *C. novyi* NT spore coat layers. Fissures first appeared (a and b) and then laterally expanded into wide gaps (c to e) and eventually resulted in the removal of whole layers, exposing the underlying layer (e and f, arrows in panel e). One expanding fissure is indicated with a white oval in panels a to f. The times in germination medium (hours:minutes) were 0:45 (a), 0:50 (b), 0:55 (c), 1:00 (d), 1:05 (e), and 1:10 (f).

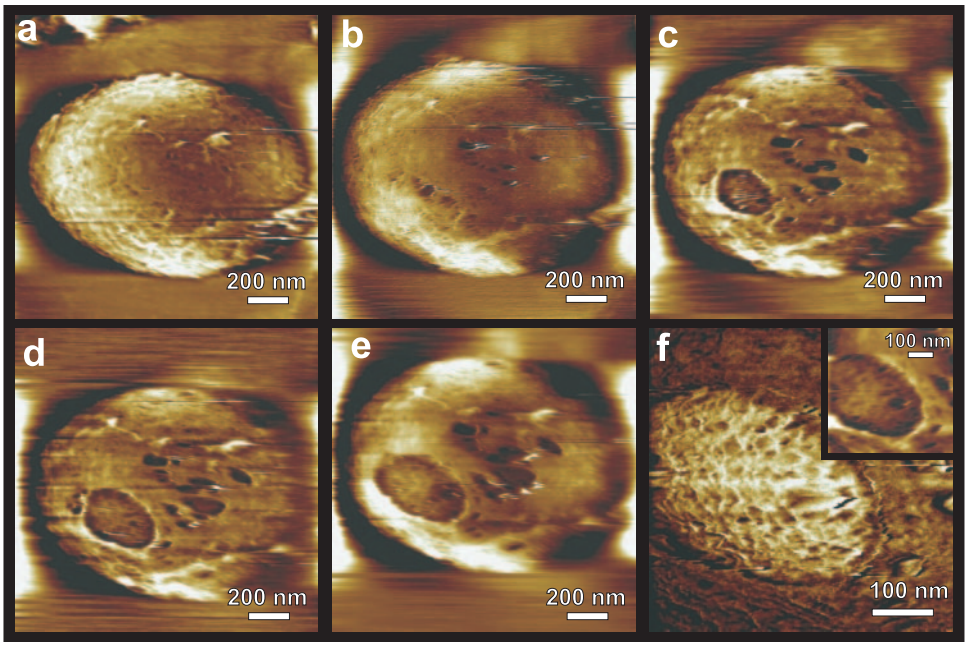

FIG. 7. (a to e) AFM height images of the final outgrowth stage. (a) After the ~6 spore coat layers were largely dissolved, the underlying structural layer was exposed. (b to e) In this layer, 25-nm deep apertures appeared and grew laterally. (f) Phase image zoom-in of the largest aperture depicted in panels c to e, showing pronounced phase contrast, indicating the different material properties of the emerging cell wall (light) and remaining spore layer (dark). The inset in panel f is the concurrent height image, showing the 25-nm deeper position of the cell wall with respect to the surrounding spore layer. The times in germination medium (hours:minutes) were 1:40 (a), 2:15 (b), 2:50 (c), 3:35 (d), 3:50 (e), and 3:55 (f).

degradation). Finally, when we did not image spores for more than an hour between two scans, the coat degradation pattern had developed similarly compared to spores that were scanned continuously.

Note that similar to our results described for germinating *B. atrophaeus* spores (41), there was a large variation in outgrowth rates for individual *C. novyi* NT spores. Thus, for some spores the degradation of the spore coat was observed as early as after 45 min of exposure to germination solution, while for other spores it could take up to several hours or not happen at all within the timeframe of observation (usually ~10 h).

When the substrate disk was rinsed and dried afterward, small amount of vegetative cells could be seen adsorbed to the substrate along with spore coat remnants (Fig. 8a and b). In Fig. 8c and d, peritrichous flagella can be seen. The flagella are attached to the cells with a hook (Fig. 8d) that is part of the bacterial flagellar motor (48). In detailed AFM images (Fig. 8d), we also observe regularly spaced, ~30-nm-wide patches with lighter phase contrast, corresponding to plateaus with an elevation of <1 nm.

DISCUSSION

From the combination of TEM and AFM images of *C. novyi* NT spores, we can construct a structural model of intact spores (Fig. 9a), as well as of germinating spores (Fig. 9b to f). From

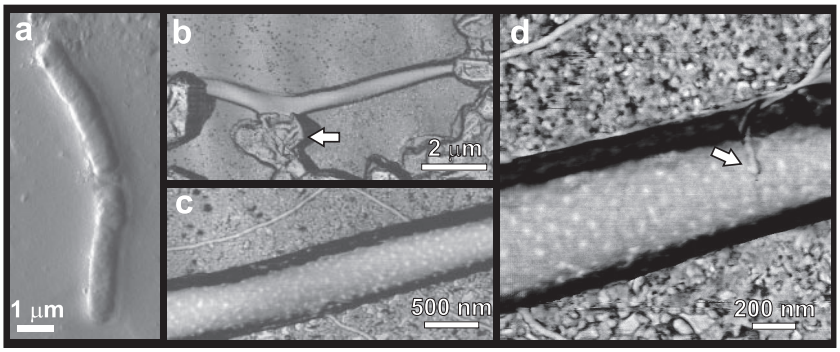

FIG. 8. AFM imaging of *C. novyi* NT vegetative cells emerging from the outgrowth experiments. (a) Typical morphology of *C. novyi* NT cells (amplitude AFM image). (b to d) AFM phase images of a *C. novyi* NT cell surrounded by spore coat remnants (arrow in panel b). In panels c and d, flagella are seen, as well as numerous, regularly spaced ~30-nm dots, which have corresponding heights of less than 1 nm. In panel d, a flagellum is seen to be attached to the cell wall with a hook (arrow). Images were taken after the sample was removed from the liquid cell, rinsed, and dried. The times in germination medium (hours:minutes) were 22:00 (a) and 17:00 (b to d).

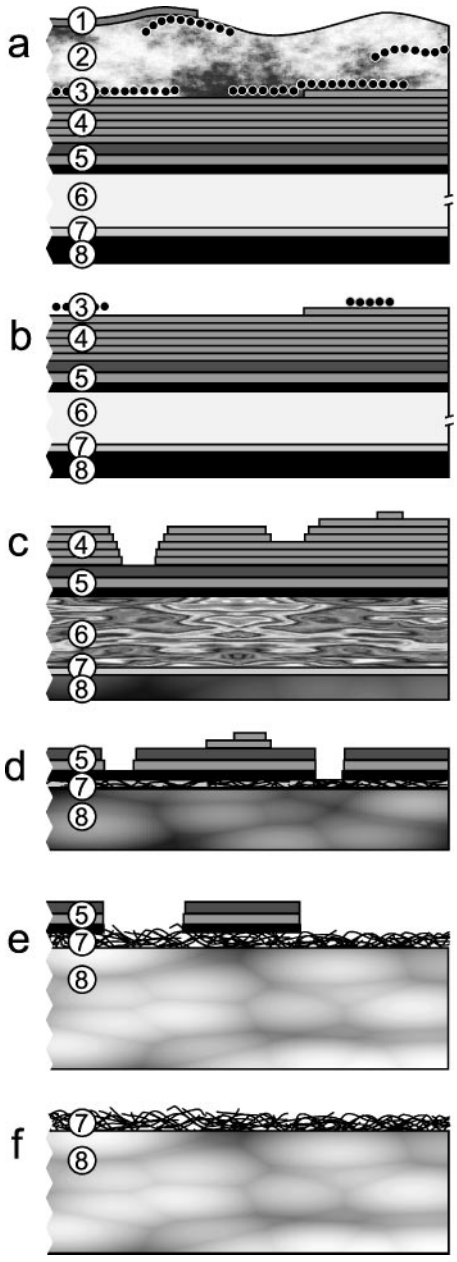

FIG. 9. Cross-section model of the *C. novyi* NT spore (a) and its evolution during the outgrowth process (b to f). (a) Circled numbers: 1, sacculus; 2, amorphous shell; 3, honeycomb layers; 4, six spore coat layers; 5, undercoat layers, consisting from three sublayers (colored gray, light, and dark); 6, cortex; 7, germ cell wall; 8, spore core. (b) At the onset of germination of shell-stripped spores, they quickly loose their remaining honeycomb layers, leaving the spore coat layers exposed (Fig. 5). (c) The spore coat layers disintegrate via widening fissures (see Fig. 6). Inside the spore, the cortex (circled 6) is lysed, while the spore core (circled 8) is starting to get transformed into a vegetative cell. (d) After the spore coat layers are removed, the undercoat layers (circled 5) are exposed on the surface (Fig. 7a and b). (e) Holes develop in the undercoat, exposing the fibrous cell wall, (Fig. 7c to f). It is unclear whether the cortex is lysed when the undercoat layers are still intact. (f) Finally, the newly formed vegetative cell (circled 8) breaks free from its spore remnants (Fig. 8).

the outside inward, the spores consist of a sacculus, an amorphous shell with intertwined honeycomb layers, often a honeycomb layer attached to the coat, approximately three to six coat layers, undercoat, cortex, germ cell wall, and the spore core. A spore outer membrane (17) may exist below the undercoat, and a spore inner membrane (17) may exist beneath the germ cell wall. However, in TEM images (Fig. 1b and c) we cannot discern these membranes from their neighboring structures (the undercoat and germ cell wall, respectively).

The amorphous shells observed for most spores could be formed by remaining cytoplasm of the mother cells that is not completely lysed during sporulation. Their relatively smooth outer edges strongly suggest that the shells are or were contained in a sacculus, which, however, is not usually observed by TEM (Fig. 1). The presence of the 50- to 100-nm-thick sacculi seen in TEM could indicate that spores were not released from their mother cell (sporangium) at the latest stages of the sporulation process and are still part of these sporangia. On the other hand, various *Bacillus* species, as well as *Clostridium botulinum* and *Clostridium bifermentans*, were found to be surrounded by a loose-fitting, balloon-like ~25- to 40-nm-thick layer, called the exosporium (17, 21, 35, 36, 38, 43, 58). In the case of *C. bifermentans* (43), the exosporium was found to contain amorphous material similar to that seen in *C. novyi* NT.

In RNA staining experiments with the RNA-specific dye SYBR green II, no appreciable fluorescence could be observed in spores and their amorphous shell while vegetative cells were green. Note that this protocol probably did not permeabilize the spore coat but should have permitted visualization of RNA in the amorphous layer if its concentration was sufficiently high. The fact that no RNA is observed in the amorphous layer as assessed by staining with the RNA-specific dye or by biochemical assays (8) supports its designation as exosporium. Since there is no evidence of a thin exosporium layer covering the amorphous shell in AFM and EM images, we conclude that the exosporia are not apparent in TEM and AFM images due to poor staining (59) or removal during processing.

Exosporia for both *Clostridium* species such as *C. botulinum* (36) and *Bacillus* species such as *B. cereus* (21, 59) and *B. thuringiensis* (59) consist of a thin, paracrystalline basal layer and an amorphous outer layer. In addition, for *B. cereus* and *B. thuringiensis*, parasporal layers are observed as single sheets or multilamellar stacks between the exosporium and the spore coat (59). Both the *Bacillus* exosporium and the parasporal layers (as well as certain *Bacillus* coat layers) have hexagonal symmetry, with periodicities ranging from 5.8 to 9.2 nm. The crystalline layers seen at different locations in the amorphous shell around *C. novyi* NT spores with TEM (Fig. 1) and AFM (Fig. 2c and 3d and e) resemble *Bacillus* parasporal layers with respect to their location, their assembly (single sheets or multilamellar), their hexagonal honeycomb structure, and their periodicity. The absence of honeycomb layers on the spore coats of a significant fraction of spores, as judged by TEM and AFM observations, the presence of the amorphous material sandwiched between the spore coat and coat-associated honeycomb layers (Fig. 1e and Fig. 3d and e), combined with the quick disappearance of these honeycomb layers during AFM germination experiments (Fig. 5), all indicate that these *C. novyi* NT honeycomb layers are not an integral part of the

spore coat, as the "pitted layer" or "honeycomb layer" is for *Bacillus* species (3, 38, 39), but rather are a parasporal layer with an increased affinity for the spore coat.

The periodicity of *C. novyi* NT honeycomb layers, as measured with AFM, is 8.7 ± 1 nm, with the closest neighbor-to-neighbor distance measured. The two-dimensional unit cell for such a hexagonal lattice is a parallelogram with an angle of 120° between the [10] (*a*) and [01] (*b*) unit cell axes of 8.7 nm in length, diagonals of 8.7 nm and $\sqrt{3} \times 8.7$ nm = 15.1 nm. In TEM thin sections, a parasporal periodicity of 15 ± 1 nm is often seen (Fig. 1). We are not sure how this relates to the honeycomb periodicity seen in AFM, but we do note that this ~15-nm periodicity is very close to the AFM-based 15.1-nm unit cell diagonal that corresponds to the next-to-closest neighbor periodicities. We speculate that when the parasporal layer is cleaved such that the [10], [01], or [11] directions are in the electron microscope's plane of view, the ~8.7-nm periodicity is so small that its crystalline character cannot be distinguished, whereas when the parasporal layer is cleaved such that the [21], [-11], or [-1-2] are seen, we *can* discern the ~15.1-nm periodicity along the unit cell diagonal.

Most germination and early outgrowth events take place within the spore and as such cannot be seen on the spore surface by AFM. The first event observable by AFM was the disassembly of the honeycomb layers residing on the spore coat (Fig. 5a and 9b). This revealed a multilayer coat structure formed by three to six visible layers with a thickness of ~6 nm each (Fig. 5b to d and Fig. 9b). While the spore coat thickness was seen to vary from 25 to 50 nm in TEM transverse sections, AFM showed this to be caused by local variations in the number of coat layers. The coat layers, formed during the sporulation stage, exhibited growth patterns (Fig. 5) typically observed on inorganic and macromolecular crystals. These patterns include steps and growth spirals originating from screw dislocations, such as those previously described in studies of the crystallization of semiconductors (9), salts (31), and biological macromolecules (32, 33). In biology, crystallization is most often associated with biomineralization, where protein-directed crystallization leads to calcious bone (56) and shell (2, 5, 53) formation. Screw dislocations and ensuing spiral growth have been observed for shell formation (51, 60). High-resolution scanning electron probe X-ray microanalysis (26, 49) and nanometer-scale secondary ion mass spectrometry (P. Weber, unpublished data) studies have demonstrated that the proteinaceous coat of several bacterial spore species is essentially devoid of divalent mineral cations such as calcium, magnesium, and manganese. This indicates that *C. novyi* NT spores could present the first case of nonmineral crystal growth patterns being revealed for a biological organism.

The implication for bacterial spore coat assembly is that, while the proteinaceous building blocks are produced via biochemical pathways directed by various enzymes and factors (17), the actual construction of these building blocks into spore coat layers is a self-assembly process similar to crystallization. Previous studies had indicated crystalline self-assembly of the rodlet and honeycomb surface layers that cover the spore coats of *Bacillus* spores (38–41) but not for the layers constituting the spore coat. In combination with the present findings, it appears that crystallization mechanisms guide the formation of inner and outer coat layers for different bacterial spore species.

The consequence of this crystalline assembly process is that the spore coat is influenced not only by the biochemical pathways leading to the production of spore coat proteins but also by the crystallization conditions during which these proteins assemble themselves. By analogy to "regular" protein crystallization, conditions during sporulation such as salt concentration, pH, the presence of impurities, and random variations in the number of screw dislocations on spores could change the growth rate and hence the thickness of the spore coat. This in turn could influence characteristics such as the resilience of spores, their lifetime, and their germination capacity.

While the presence of the above mentioned growth patterns strongly points to a crystalline nature of the coat layers, detailed AFM observations did not result in the visualization of a crystalline lattice. Hence, the lattice periodicity is assumed to be smaller than ~1 nm, which is the resolution associated with the sharpest AFM tips used. Such a periodicity would be small compared to the 6-nm thickness of individual spore coat layers. In the case of globular proteins, lateral lattice parameters typically do not differ to such an extent from the height of growth layers, which is reflected in relatively small differences between lateral and perpendicular crystallographic unit cell parameters (29). Thus, the proteins forming the *C. novyi* NT crystalline spore coat layers are likely not globular but rather may be stretched peptides "standing upright" in the layers. This construction, which is found in paraffin (42) and fat crystals (25), results in a crystal class with relatively strong, hydrophobic interaction forces between the long neighboring units (here peptides) and weak interaction forces between the different crystalline layers. This generally leads to wide, thin crystals that mainly grow laterally and can grow perpendicular only via the screw dislocation spiral mechanism (as was indeed seen for the *C. novyi* NT coat layers). Such a crystal type, with tightly packed, strongly interacting longitudinal peptides within a layer, would help explain the toughness associated with bacterial spore coats (3, 17). It may also explain why spore coat proteins are difficult to dissolve (3, 17, 19, 28), since this type of packing involves hydrophobic interactions and hence a high proportion of hydrophobic amino acids.

In addition to enabling the nucleation and growth of new coat layers during sporulation, the screw dislocations also pin several of these layers together, thereby making the spore coat an interconnected, cohesive entity, rather than a set of separate layers loosely deposited on top of each other. This, combined with the strong in-layer bonds and possible cross-linking between the coat proteins, likely contributes to the resilient nature of the spore coat.

As seen in Fig. 6, the spore coat layers slowly degenerate by fissure formation, followed by slow dissolution of the resulting steps (Fig. 6 and 9c and d). Later stages of coat degradation likely take place during the outgrowth stage, while the initial formation of fissures (Fig. 6a) could take place during the last stages of spore germination. Spore coat degradation likely occurs under the influence of germination-activated lytic enzymes. Such lytic enzymes are known to be encoded within the *C. novyi* NT genome (8). Interestingly, *C. novyi* NT spores contain mRNA, and these mRNA molecules are enriched in proteins that could assist with cortex and other degradation (8). The structure seen below the approximately six coat layers (Fig. 6d to f, 7a, and 9c to e) most likely corresponds to the

three undercoat layers observed by TEM, which were determined to have a total 18- to 26-nm thickness (Fig. 1b). The cortex was fully lysed by the time these layers dissolved. Therefore, the flat-bottom apertures in this undercoat layer show the underlying cell wall of the emerging *C. novyi* NT vegetative cell, which, based on its lighter AFM phase contrast (Fig. 7f), has different physicochemical properties and hence a different composition than the surrounding coat remnants. The nascent surface of the emerging germ cell appears to be formed by a porous network (Fig. 7f and 9e and f). Similar networks of peptidoglycan fibers were recently reported in AFM studies of *Staphylococcus aureus* (50) and *B. atrophaeus* vegetative cells (41).

Imaging of air-dried cells adhered to the substrate revealed flagella in a peritrichous scheme, attached to the cell walls with a hook (48). Based on their regular spacing, we believe that the white spots observed on the cell walls in AFM tapping-mode phase images (Fig. 8c and d) are an integral part of the *C. novyi* NT cell wall, although at this point we do not know their constitution or function.

Furthermore, we found that heat activation for 0.5 h at 70 or 80°C dramatically accelerated spore germination, without observable spore degeneration. The evaluation of the role of heat activation in in vivo germination is of particular importance for bacteriolytic therapies. After heat activation, most spores (>90%) germinated within the timeframe of the observations, i.e., they turned dark in phase-contrast microscopy experiments. A significant fraction (<30%) of the spores did not proceed to the final outgrowth stage, i.e., germ cell emergence, during observation and did not exhibit degradation of the spore coat layer. In AFM experiments, these germinated spores showed a structural collapse after the sample was dried, indicating the prior replacement of the dipicolinic acid inside the core with water. Possibly, the germination medium allowed rapid initiation of spore germination but did not have sufficient nutritional resources to allow extensive vegetative cell outgrowth. Alternatively, the medium may not be able to maintain a low enough oxygen level for more widespread outgrowth.

In conclusion, we have shown that the correlative use of ultrathin-section TEM and AFM provides detailed information on the architecture of the outer layers of *C. novyi* NT spores. Direct observation of the spiral growth patterns suggests that spore coat construction is a self-assembly process similar to the formation of conventional and macromolecular crystals. It therefore is subject to the chemical environment and thermodynamic parameters that generally control crystallization. The densely packed crystalline peptide assembly may explain the material strength and resilience of bacterial spore coats. Increased knowledge of spore coat architecture and the germination process could help direct future genetic modifications of *C. novyi* NT for use in tumor therapy.

ACKNOWLEDGMENTS

This study was performed under the auspices of the U.S. Department of Energy by the University of California, Lawrence Livermore National Laboratory under contract W-7405-Eng-48. This study was supported by the Lawrence Livermore National Laboratory through Laboratory Directed Research and Development Grant 04-ERD-002, the Miracle Foundation, the Commonwealth Foundation, and NIH grant CA 62924.

REFERENCES

1. **Agrawal, N., C. Bettegowda, I. Cheong, J.-F. Geschwind, C. G. Drake, E. L. Hipkiss, M. Tatsumi, L. H. Dang, L. A. Diaz, Jr., M. Pomper, M. Abusedera, R. L. Wahl, K. W. Kinzler, S. Zhou, D. L. Huso, and B. Vogelstein.** 2004. Bacteriolytic therapy can generate a potent immune response against experimental tumors. Proc. Natl. Acad. Sci. USA **101:**15172–15177.
2. **Aizenberg, J., G. Lambert, S. Weiner, and L. Addadi.** 2002. Factors involved in the formation of amorphous and crystalline calcium carbonate: a study of an ascidian skeleton. J. Am. Chem. Soc. **124:**32–39.
3. **Aronson, A. I., and P. Fitz-James.** 1976. Structure and morphogenesis of the bacterial spore coat. Bacteriol. Rev. **40:**360–402.
4. **Bagadi, H. O., and M. M. H. Sewell.** 1973. Experimental studies of infectious necrotic hepatitis (black disease of sheep). Res. Vet. Sci. **15:**53–61.
5. **Belcher, A. M., X. N. Wu, R. J. Christensen, P. K. Hansma, G. D. Stucky, and D. E. Morse.** 1996. Control of crystal phase switching and orientation by soluble mollusc-shell proteins. Nature **381:**56–58.
6. **Bette, P., J. Frevert, F. Mauler, N. Suttorp, and E. Habermann.** 1989. Pharmacological and biochemical studies of cytotoxicity of *Clostridium-novyi* type a alpha-toxin. Infect. and Immunol. **57:**2507–2513.
7. **Bettegowda, C., L. H., R. Dang, D. L. Abrams, L. Huso, I. Dillehay, N. Cheong, N. Agrawal, S. Borzillary, J. M. McCaffery, E. L. Watson, K. S. Lin, F. Bunz, K. Baidoo, M. G. Pomper, K. W. Kinzler, B. Vogelstein, and S. Zhou.** 2003. Overcoming the hypoxic barrier to radiation therapy with anaerobic bacteria. Proc. Natl. Acad. Sci. USA **100:**15083–15088.
8. **Bettegowda, C., X. Huang, J. Lin, I. Cheong, M. Kohli, S. A. Szabo, X. S. Zhang, L. A. Diaz, V. E. Velculescu, G. Parmigiani, K. W. Kinzler, B. Vogelstein, and S. Zhou.** 2006. The genome and transcriptomes of the anti-tumor agent *Clostridium novyi* NT. Nat. Biotechnol. **24:**1573–1580.
9. **Brar, B., and D. Leonard.** 1994. Spiral growth of GaSb on (001) GaAs using molecular beam epitaxy. Appl. Phys. Lett. **66:**463–465.
10. **Cabrera, N., and M. M. Levine.** 1956. On the dislocation theory of evaporation of crystals. Philos. Mag. **1:**450–458.
11. **Cano, R. J., and M. K. Borucki.** 1995. Age of bacteria from amber-response. Science **268:**1060–1064.
12. **Cheong, I., X. Huang, C. Bettegowda, L. A. Diaz, Jr., K. W. Kinzler, S. Zhou, and B. Vogelstein.** 2006. A bacterial protein enhances the release and efficacy of liposomal cancer drugs. Science **314:**1308–1311.
13. **Dang, L. H., C. Bettegowda, D. L. Huso, K. W. Kinzler, and B. Vogelstein.** 2001. Combination bacteriolytic therapy for the treatment of experimental tumors. Proc. Natl. Acad. Sci. USA **98:**15155–15160.
14. **DeYoreo, J. J., T. A. Land, and B. Dair.** 1994. Growth morphology of vicinal hillocks on the (101) face of KH_2PO_4 from step-flow to layer-by-layer growth. Phys. Rev. Lett. **73:**838–841.
15. **DeYoreo, J. J., T. A. Land, and J. D. Lee.** 1997. Limits on surface vicinality and growth rate due to hollow dislocation cores on KDP {101}. Phys. Rev. Lett. **78:**4462–4465.
16. **Diaz, L. A., Jr., I. Cheong, C. A. Foss, X. A. Zhang, B. A. Peters, N. Agrawal, C. Bettegowda, B. Karim, G. S. Liu, K. Khan, X. Huang, M. Kohli, L. H. Dang, P. Hwang, A. Vogelstein, E. Garrett-Mayer, B. Kobrin, M. Pomper, S. Zhou, K. W. Kinzler, B. Vogelstein, and D. L. Huso.** 2005. Pharmacologic and toxicologic evaluation of *C. novyi* NT spores. Toxicol. Sci. **88:**562–575.
17. **Driks, A.** 1999. *Bacillus subtilis* spore coat. Microbiol. Mol. Biol. Rev. **63:**1–21.
18. **Dufrêne, Y. F.** 2004. Using nanotechnologies to explore microbial surfaces. Nat. Rev. Microbiol. **2:**451–458.
19. **Freiben, W. R., and C. L. Duncan.** 1973. Homology between enterotoxin protein and spore structural protein in *Clostridium perfringens* type A. Eur. J. Biochem. **39:**393–401.
20. **Frese, R. N., C. A. Siebert, R. A. Niederman, C. N. Hunter, C. Otto, and R. van Grondelle.** 2004. The long-range organization of a native photosynthetic membrane. Proc. Natl. Acad. Sci. USA **101:**17994–17999.
21. **Gerhard, P., and E. Ribi.** 1964. Ultrastructure of the exosporium enveloping spores of *Bacillus cereus*. J. Bacteriol. **88:**1774–1789.
22. **Hatheway, C. L.** 1990. Toxigenic clostridia. Clin. Microbiol. Rev. **3:**66–98.
23. **Hinterdorfer, P., and Y. F. Dufrêne.** 2006. Detection and localization of single molecular recognition events using atomic force microscopy. Nat. Methods **3:**347–355.
24. **Hoh, J. H., R. Lal, S. A. John, J. P. Revel, and M. F. Arnsdorf.** 1991. Atomic force microscopy and dissection of gap-junctions. Science **253:**1405–1408.
25. **Hollander, F. F. A., M. Plomp, C. J. van de Streek, and W. J. P. van Enckevort.** 2001. A two-dimensional Hartman-Perdok analysis of polymorphic fat surfaces observed with atomic force microscopy. Surf. Sci. **471:**101–113.
26. **Johnstone, K., D. J. Ellar, and T. C. Appleton.** 1980. Location of metal ions in *Bacillus megaterium* spores by high resolution electron probe X-ray microanalysis. FEMS Microbiol. Lett. **7:**97–101.
27. **Karrasch, S. R., R. Hegerl, J. H. Hoh, W. Baumeister, and A. Engel.** 1994. Atomic force microscopy produces faithful high-resolution images of protein surfaces in aqueous environment. Proc. Natl. Acad. Sci. USA **91:**836–838.
28. **Kim, H.-S., D. Sherman, F. Johnson, and A. I. Aronson.** 2004. Character-

ization of major *Bacillus anthracis* spore coat protein and its role in spore inactivation. J. Bacteriol. **186:**2413–2417.
29. **Kuznetsov, Yu. G., A. J. Malkin, T. A. Land, J. J. DeYoreo, A. P. Barba, J. Konnert, and A. McPherson.** 1997. Molecular resolution imaging of macromolecular crystals by atomic force microscopy. Biophys. J. **72:**2357–2364.
30. **Maganov, S. N.** 2000. AFM analysis of polymers, p. 7432–7491. *In* R. A. Meyers (ed.), Encyclopedia of analytical chemistry. John Wiley & Sons, Ltd., Chichester, United Kingdom.
31. **Maiwa, K., M. Plomp, W. J. P. van Enckevort, and P. Bennema.** 1998. AFM observation of barium nitrate {111} and {100} faces: spiral growth and two-dimensional nucleation growth. J. Crystal. Growth **186:**214–223.
32. **Malkin, A. J., Yu. G. Kuznetsov, T. A. Land, J. J. DeYoreo, and A. McPherson.** 1995. Mechanisms of growth for protein and virus crystals. Nat. Struct. Biol. **2:**956–959.
33. **Malkin, A. J., and A. McPherson.** 2004. Probing of crystal interfaces and the structures and dynamic properties of large macromolecular ensembles with in situ atomic force microscopy, p. 201–238. *In* X. Y. Lin and J. J. DeYoreo (ed.), From solid-liquid interface to nanostructure engineering, vol. 2. Plenum/Kluwer Academic Publishers, New York, NY.
34. **Malkin, A. J., A. McPherson, and P. D. Gershon.** 2003. Structure of intracellular mature vaccinia virus visualized by in situ AFM. J. Virol. **77:**6332–6340.
35. **Moir, A.** 2006. How do spores germinate? J. Appl. Microbiol. **101:**526–530.
36. **Montville, T. J., S. B. Jones, L. K. Conway, and G. M. Sapers.** 1985. Germination of spores from *Clostridium botulinum* B-aphis and Ba410. Appl. Environ. Microbiol. **50:**795–800.
37. **Muller, D., and A. Engel.** 1999. Voltage and pH-induced channel closure of porin OmpF visualized by atomic force microscopy. J. Mol. Biol. **285:**1347–1351.
38. **Plomp, M., T. J. Leighton, K. E. Wheeler, and A. J. Malkin.** 2005. The high-resolution architecture and structural dynamics of *Bacillus* spores. Biophysical J. **88:**603–608.
39. **Plomp, M., T. J. Leighton, K. E. Wheeler, and A. J. Malkin.** 2005. Architecture and high-resolution structure of *Bacillus thuringiensis* and *Bacillus cereus* spore coat surfaces. Langmuir **21:**7892–7898.
40. **Plomp, M., T. J. Leighton, K. E. Wheeler, M. E. Pitesky, and A. J. Malkin.** 2005. *Bacillus atrophaeus* outer spore coat assembly and ultrastructure. Langmuir **21:**10710–10716.
41. **Plomp, M., T. J. Leighton, K. E. Wheeler, H. D. Hill, and A. J. Malkin.** 2007. In vitro high-resolution structural dynamics of single germinating bacterial spores. Proc. Natl. Acad. Sci. USA **104:**9644–9649.
42. **Plomp, M., W. J. P. van Enckevort, P. J. C. M. van Hoof, and C. J. van de Streek.** 2003. Morphology and dislocation movement in n-$C_{40}H_{82}$ paraffin crystals grown from solution. J. Crystal. Growth **249:**600–613.
43. **Pope, L., D. P. Yolton, and L. J. Rode.** 1967. Appendages of *Clostridium bifermentans* spores. J. Bacteriol. **94:**1206–1215.
44. **Raju, D., P. Setlow, and M. R. Sarker.** 2007. Antisense-RNA-mediated decreased synthesis of small, acid-soluble spore proteins leads to decreased resistance of *Clostridium perfringens* spores to moist heat and UV radiation. Appl. Environ. Microbiol. **73:**2048–2053.
45. **Schabert, F. A., C. Henn, and A. Engel.** 1995. Native *Escherichia coli* OmpF surfaces probed by atomic force microscopy. Science **268:**92–94.
46. **Setlow, P.** 2003. Spore germination. Curr. Opin. Microbiol. **6:**550–556.
47. **Setlow, P.** 2006. Spores of *Bacillus subtilis*: their resistance to and killing by radiation, heat and chemicals. J. Appl. Microbiol. **101:**514–525.
48. **Sowa, Y., A. D. Rowe, M. C. Leake, T. Yakushi, M. Homma, A. Ishijima, and R. M. Berry.** 2005. Direct observation of steps in rotation of the bacterial flagellar motor. Nature **437:**916–919.
49. **Stewart, M., A. P. Somlyo, A. V. Somlyo, H. Shuman, J. A. Lindsay, and W. G. Murrell.** 1980. Distribution of calcium and other elements in cryosectioned *Bacillus cereus* T spores, determined by high-resolution scanning electron probe X-ray microanalysis. J. Bacteriol. **143:**481–491.
50. **Touhami, A., M. H. Jericho, and T. J. Beveridge.** 2004. Atomic force microscopy of cell growth and division in *Staphylococcus aureus*. J. Bacteriol. **186:**3286–3295.
51. **Yao, N., A. Epstein, and A. Akey.** 2006. Crystal growth via spiral motion in abalone shell nacre. J. Materials Res. **21:**1939–1946.
52. **Yau, S. T., D. N. Petsev, B. R. Thomas, and P. G. Vekilov.** 2000. Molecular-level thermodynamic and kinetic parameters for the self-assembly of apoferritin molecules into crystals. J. Mol. Biol. **303:**667–678.
53. **Young, J. R., and K. Hendriksen.** 2003. Biomineralization within vesicles: the calcite of coccoliths, p. 189–215. *In* P. M. Dove, J. J. De Yoreo, and S. Weiner (ed.), Reviews in mineralogy and geochemistry, vol. 54. Mineralogical Society of America, Washington, DC.
54. **Van der Hoek, B., J. P. Van der Eerden, and P. Bennema.** 1982. Thermodynamical stability conditions for the occurrence of hollow cores caused by stress of line and planar defects. J. Crystal Growth **56:**621–632.
55. **Van Mellaert, L., S. Barbé, and J. Anné.** 2006. *Clostridium* spores as anti-tumour agents. Trends Microbiol. **14:**190–196.
56. **Veis, A.** 2003. Mineralization in organic matrix networks, p. 249–289. *In* P. M. Dove, J. J. De Yoreo, and S. Weiner (ed.), Reviews in mineralogy and geochemistry, vol. 54. Mineralogical Society of America, Washington, DC.
57. **Vreeland, R. H., W. D. Rosenzweig, and D. W. Powers.** 2000. Isolation of a 250 million-year-old halotolerant bacterium from a primary salt crystal. Nature **407:**897–900.
58. **Waller, L. N., N. Fox, K. F. Fox, A. Fox, and R. L. Price.** 2004. Ruthenium red staining for ultrastructural visualization of a glycoprotein layer surrounding the spore of *Bacillus anthracis* and *Bacillus subtilis*. J. Microbiol. Methods **58:**23–30.
59. **Wehrli, E., P. Scherrer, and O. Kübler.** 1980. The crystalline layers in spores of *Bacillus cereus* and *Bacillus thuringiensis* studied by freeze-etching and high resolution electron microscopy. Eur. J. Cell Biol. **20:**283–289.
60. **Wise, S. W., and J. deVilliers.** 1971. Scanning electron microscopy of molluscan shell ultrastructures: screw dislocations in pelecypod nacre. Trans. Am. Microbiol. Soc. **90:**376–380.